ORIGINAL ARTICLE

CrossMark

Laser-induced plasma spectroscopy (LIPS): use of a geological tool in assessing bone mineral content

László Andrássy[1] · Izabella Gomez[2] · Ágnes Horváth[2] · Katalin Gulyás[2] · Zsófia Pethö[2] · Balázs Juhász[3] · Harjit Pal Bhattoa[4] · Zoltan Szekanecz[2]

Abstract

Bone may be similar to geological formulations in many ways. Therefore, it may be logical to apply laser-based geological techniques in bone research. The mineral and element oxide composition of bioapatite can be estimated by mathematical models. Laser-induced plasma spectrometry (LIPS) has long been used in geology. This method may provide a possibility to determine the composition and concentration of element oxides forming the inorganic part of bones. In this study, we wished to standardize the LIPS technique and use mathematical calculations and models in order to determine CaO distribution and bone homogeneity using bovine shin bone samples. We used polished slices of five bovine shin bones. A portable LIPS instrument using high-power Nd++YAG laser pulses has been developed (OpLab, Budapest). Analysis of CaO distribution was carried out in a 10×10 sampling matrix applying 300-μm sampling intervals. We assessed both cortical and trabecular bone areas. Regions of interest (ROI) were determined under microscope. CaO peaks were identified in the 200–500 nm wavelength range. A mathematical formula was used to calculate the element oxide composition (wt%) of inorganic bone. We also applied two accepted mathematical approaches, the Bartlett's test and frequency distribution curve-based analysis, to determine the homogeneity of CaO distribution in bones. We were able to standardize the LIPS technique for bone research. CaO concentrations in the cortical and trabecular regions of B1–5 bones were $33.11 \pm 3.99\%$ (range 24.02–40.43%) and $27.60 \pm 7.44\%$ (range 3.58–39.51%), respectively. CaO concentrations highly corresponded to those routinely determined by ICP-OES. We were able to graphically demonstrate CaO distribution in both 2D and 3D. We also determined possible interrelations between laser-induced craters and bone structure units, which may reflect the bone structure and may influence the heterogeneity of CaO distributions. By using two different statistical methods, we could confirm if bone samples were homogeneous or not with respect to CaO concentration distribution. LIPS, a technique previously used in geology, may be included in bone research. Assessment of element oxide concentrations in the inorganic part of bone, as well as mathematical calculations may be useful to determine the content of CaO and other element oxides in bone, further analyze bone structure and homogeneity and possibly apply this research to normal, as well as diseased bones.

Keywords Laser-induced plasma spectrometry · LIPS · Element oxide · CaO · Mathematical model · Bioapatite · Bartlett's test · Frequency characteristic · Homogeneity

✉ Zoltan Szekanecz
   szekanecz.zoltan@med.unideb.hu; https://www.rheumatology.hu

1   Hungarian Geological and Geophysical Institute, Budapest, Hungary

2   Department of Rheumatology, Faculty of Medicine, University of Debrecen, Nagyerdei Str 98, Debrecen H-4032, Hungary

3   Department of Oncology, Faculty of Medicine, University of Debrecen, Debrecen, Hungary

4   Department of Laboratory Medicine, Faculty of Medicine, University of Debrecen, Debrecen, Hungary

Introduction

The dry matter of bone contains both organic and inorganic constituents. The proportion and distribution of inorganic constituents changes with growth, the aging process and in diseases, such as osteoporosis [1]. The inorganic part of bone is approx. 49% [2].

In the human and animal bone tissues, most of the normal and pathological constituents are calcium phosphate-type minerals, which are members of the apatite series.

The most acceptable formula to describe biopatites is as follows:

$$(Ca, Mg, Na, [])_{10}(PO_4, HPO_4, CO_3)_6(OH, F, Cl, CO_3, O_2, [])_2$$
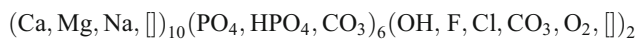
In addition to the normal composition, metals, trace elements and sometimes toxic ingredients may be deposited to the bone. Aluminum (Al) may be accumulated in individuals taking antacids, as well as in patients undergoing dialysis [3, 4]. Al may suppress bone mineralization leading to renal osteodystrophy [5]. Al has been replaced by lanthanum (La) as a phosphate-binding element. La may be deposited into the bone and caused reversible mineralization defects in rats [4, 6]. Cadmium (Cd) may cause renal tubular dysfunction, osteomalacia and nephrocalcinosis and may increase bone fracture risk as it antagonizes calcium and vitamin D absorption [4, 7]. Acute lead (Pb) toxicity can be detected from blood; however, cumulative toxicity may be determined by bone biopsy [8]. Pb inhibits bone development including osteoblast differentiation, as well as fracture healing [4, 9]. Lithium (Li) salts, still used to treat depression, causes hyperparathyroidism and bone loss [10, 11]. Yet, long-term Li intake was not associated with increased osteoporosis risk [12]. Excessive iron (Fe) intake associated with thalassemia, hemochromatosis or sickle cell disease often results in osteoporosis due to the suppression of osteoblast functions [4, 13]. Trace elements, such as zinc (Zn) [14, 15], copper (Cu) [15], magnesium (Mg) [16] and manganese (Mn) [4] are natural ingredients of bone and are needed for bone physiology. In this case, low levels in bone, rather than toxicity may be relevant [4]. Finally, strontium (Sr) ranelate is an available anti-osteoporotic agent that inhibits osteoclasts and stimulates osteoblasts. The assessment of Sr in bone by non-invasive methods may be useful to monitor drug accumulation [4, 17, 18]. Thus, there may be a need in medicine to assess these elements in the bone.

The assessment of bone structure and bone content may be essential in various bone and calcium homeostasis disorders [19]. Bone densitometry (DEXA) has been widely used to determine bone density in osteoporosis and other conditions [19]. Bone structure may be assessed by micro-CT or high-resolution MRI techniques [19, 20]. Yet, the assessment of bone mineral content and the concentration of various elements in the bone have not yet been elucidated. Bone biopsy has been the standard method for studying bone structure and composition. For example, D'Haese et al. [21] assessed numerous metals and trace elements in 100 bone biopsy samples taken from patients with renal failure. The levels of Al and Cd were highly increased in the bone of end-stage uremic patients. Bone Al, Pb and Sr constant was especially high in patients with osteomalacia. This is rather painful and not all individuals may be biopsied [19]. Therefore, it is evident that bone biopsy will never become a routinely used diagnostic test [19].

These issues lead to the idea to apply geological techniques to bone research. Indeed, inorganic minerals are the most abundant constituents of bones. Laser-based techniques, for example inductively coupled plasma mass spectrometry (ICP-MS) have been long used in geology for elemental determinations. Few groups have applied ICP-MS for bone and dental research. For example, Uryu et al. [22] applied laser ablation ICP-MS for the determination of Pb in teeth. Hetter et al. [23] standardized ICP-MS for the assessment of Pb in animal bones. Liu et al. [24] took human rib homogenates and applied plasma MS to determine elements of the La group. Raffalt et al. [25] could detect Sr incorporation into canine bones and tooth enamel following Sr treatment. Finally, in archaeology, Shafer et al. [26] used ICP-MS to measure trace elements in bones from the Iron Age. They found increased incorporation of Mn, Cd and Ni on the bony surface. As described above, mostly ICP-MS, a rather complex and costly technique has been used in most studies.

Laser-induced plasma spectrometry (LIPS) has long been used in the Geological and Geophysical Institute of Hungary (GGIH), Budapest. In LIPS, high-power density (109–1012 W/cm^2) laser beam is focused on a small-sized target surface (40–60 μm in diameter). The atoms in the generated vapour are excited to produce spectral lines. By resolving the emitted radiation, a spectrum is observed for the determination of elemental composition. On the other hand, laser ablation inductively coupled plasma mass spectrometry (LA-ICP-MS) enables identification and comparison of physical evidence, discriminating elemental and isotopic differences at the part per billion (ppb) level. In contrast to aqueous analysis, where significant amounts of material need to be destroyed, in LA-ICP-MS, the sample particles are transported to ICP-MS and atomization, as well as excitation occur in ICP [27]. The construction of portable LIPS systems is a hot research topic. Primarily, space research and military applications have been published; however, geological applications are also important [27]. A LIPS instrument linked to the ImaGeo Corescanner was developed at GGIH in the late 1990s [28] and has been used in many geological studies for measuring the spatial distribution of structures and geological phenomena in drill cores at various sites of Hungary as well as in international collaborations [29–31]. However, the LIPS technique has not yet been introduced to the field of bone research. Therefore, we wished to apply LIPS to bone by using a mathematical model approaching the inorganic content of normal mineralized animal bone tissue. Furthermore, before the application of the LIPS technique to human bones, a baseline study carried out in animal bones was necessary in order to characterize chemical and mineralogical/organic composition of bones and to develop a protocol for further human bone assessments.

Thus, bone research and geology may complement each other and this may open a new perspective for the

development and application of new laser-based geological techniques to study the chemical composition of bones.

Materials and methods

Bovine bone samples

A total of five male bovine tibial (B1–B5) bone samples were used for the initial characterization. The organic matter (meat and marrow) was removed from the bones first mechanically and then by boiling in water with 1% hydrogen peroxide. The bones were cut into slices using a diamond saw, and then thin polished bone slices were prepared for LIPS. Polishing was performed under dry conditions. First, one side of the slice was polished and glue attached to microscope slides. Then, the other side was carefully polished. This surface must be smooth enough for LIPS measurements.

LIPS instrument and technique

A LIPS instrument (OpLab, Budapest, Hungary) has been developed and used. The major characteristics of the instrument (detection setup and spectroscopic system) are as follows.

Regarding the detection setup, the W power, the Φ flux and the I power density of the laser impulse are calculated as follows:

$$W = E/\tau, \Phi = E/d_0 \text{ and } I = W/d_0$$

where

W Laser impulse power ($19.5 \times 10^{-3}/4 \times 10^{-9} = 4.875 \times 10^6$ J/s);
Φ Laser impulse flux (J/cm^2);
I Laser impulse power density (W/cm^2);
E Laser impulse energy (19.5×10^{-3} J);
τ Laser impulse time period ($4 \text{ ns} = 4 \times 10^{-9}$ s);
d_0 Laser bundle-derived spot diameter in focal plain.

In the focal plain, the d_0 diameter of the spot is calculated as follows:

$$d_0 = 4 \lambda f/\pi D$$

where

d_0 Laser bundle-derived spot diameter in focal plain;
D Laser bundle diameter on the lens (3 mm);
λ Laser wavelength (1064 nm);
f focal length.

Thus, if focal length (f) is 25 mm, $d_0 = 0.011$ mm, laser beam-derived spot area in focal plain (A) = 0.000099 mm^2, $I = 4.9 \times 10^8$ W/cm^2 and $\Phi = 1.947$ J/cm^2.

With respect to the spectroscopic system, the medium resolution was 0.5 nm. We used a Hamamatsu NMOS linear image sensor (1″ 1024 pixels), product code: S3904-1024Q (Hamamatsu Photonics Inc.), a Chemspec 100S polychromator (American Holographic Inc.), and an MK367 1064 nm ND:YAG laser head (Kigre Inc.). In principle, a high-power Nd++YAG laser pulse hits the sample under examination and produces plasma. The light, coming from the plasma is focused onto the circular endface of a fibre optics bundle by a quartz optical system. This bundle guides the light to a holographic concave polychromator. The spectrum is detected by a diode array. A 16-bit AD processes the resulted analogue signal and, in turn, data will be transferred (through an RS 232 interface) to an external PC where analysis of the spectrum is performed. The installed software also provides control functions to the system [28, 30, 32].

Thin polished bone slides prepared from male bovine tibia as described above were examined under a LIPS instruments. The LIPS protocol and sampling technique were established in the present study, thus, they are described in the 'Results' section. As the polishing material may interfere with the detection of elements, rough-grained carborundum (SiC) and then fine-particle aluminium-oxide were used for rough and fine polishing, respectively. CaO concentrations were detected at 393.4-nm wavelength (λ), which yields the most striking spectrum line. This does not interfere with Al, C, and Si spectrum lines.

The LIPS software uses a standard element library composed of data from typical matrix and trace elements as previously determined from reference samples in various wavelength ranges. The standard element library contains those elements, which may be of medical relevance and others that may find application in various research fields. We used a LIPS standard element library in wavelength ranges of 200–500 and 500–800 nm, respectively.

Mathematical determination of elemental oxide and elemental concentrations

In order to determine element/element oxide concentrations in the inorganic part of the bone, a separate calibration function was generated for each element. Calibration was enabled by using commercially available element standards containing variable element concentrations. Emission spectra were analysed, the most striking interference-free spectrum-lines were evaluated and the peak amplitudes were determined. Integral normalized, mixed normalized (V1 and V5) and mixed integral normalized peak amplitude values were taken as input data for further regression analysis.

Five different regression functions were used:

Power function (Malpica) $I = P_3 \times c^{P2 \times c}$
Exponential function $I = P_3 \times \exp.(P_2 \times c)$

Logarithmic function $I = P_1 \times \log(c) + P_0$
Linear function $I = P_1 \times c + P_0$
Quadric polynomial function $I = P_3 \times c^2 + P_2 \times c + P_0$

where

I	Spectrum-line peak amplitude values;
P_0, P_1, P_2 and P_3	Parameter vectors determined during calibration;
c	Elemental oxide concentration.

Finally, elemental concentrations were calculated. Considering the atomic weight (AW) of elements, molecular weight (MW) values of the elemental oxides (molecules) were determined. Then, the MW/AW 'constant' was calculated. Elemental concentration can be calculated by taking the quotient of elemental oxide concentration and the constant.

Statistical analysis

LIPS measurements values are presented as mean $\% \pm SD$. Comparison of bone homogeneity was performed by using the Bartlett's test [33] and χ^2 test (described later in detail). The mathematical modelling of inorganic element concentrations in the bone is also described in detail later.

Results

Mathematical modelling of the inorganic compartment of the bone tissue

The structural similarities between the inorganic component of bone tissue and geological formations suggest that mathematical models may be used to determine weight percentage composition of the different mineral element oxides constituting the inorganic component of bone tissue [31]. The determined weight percentage composition can be verified with the determination of element oxide concentration values by LIPS and ICP-OES/MS. It can be concluded from calculated weight percentage composition of the inorganic component of bone tissue and laboratory analyses that the properties of bone tissue are determined primarily by hydroxyl apatite [2].

The below described formula should be used to calculate the element oxide weight percentage (wt%) composition of the mineral constituents in the inorganic component [31]:

$$[MP] \times [MW] \times [MN] = [CMW]$$

where

MP	Mass percentage;
MW	Molecular weight;
MN	Molecular number;
CMW	Corrected molecular weight.

Element oxide concentration values can be presented as weight percentage when the corrected molecular weight of each mineral component are known:

$$[C_o] = [CMW] \times [\rho_{mineral}]/[MW_{mineral}]/[\rho_{bone\ tissue}]$$

where

C_o	Element oxide concentration (weight percentage);
$\rho_{mineral}$	Density of the mineral constituents in the inorganic component;
$\rho_{bone\ tissue}$	Bone tissue density by laboratory assessment;
$MW_{mineral}$	Molecular weight of the mineral constituents in the inorganic component.

An example of the mathematical modelling of the mineral constituents in the inorganic component of bone tissues is shown in Table 1. C_o can be computed from CMW, $MW_{mineral}$, $\rho_{mineral}$ and $\rho_{bone\ tissue}$. Bone tissue density can be determined in a laboratory or can be an estimated value.

The weight percentage composition of the mineral constituents in the inorganic component of bone tissue was determined by mathematical modelling. We assessed the composition of the oxides as determined by the ICP-OES technique, and the concentration values of the organic component, water and CO_2 were determined by thermogravimetry (data not shown). These methods are routinely available at the GGIH.

With the help of the mathematical modelling, the element oxide (C_o) concentration values and water content of bioapatite are presented in Table 2. From this, the concentrations of elements (C_e) can be calculated and compared with the published concentration values [2]. As presented in Table 2, there is a high degree of agreement between the calculated and published C_e (%) values, except for CO_2.

It may be concluded from the mathematical modelling of the weight percentage of the mineral constituents in bone, as well as from the laboratory measurements performed on the bovine shin bones, that the properties of the bone tissue are primarily determined by its hydroxylapatite content. Since hydroxylapatite is constituted by CaO, P_2O_5 oxides and bound water, the bone structure can be investigated by measurement of CaO distribution by the LIPS technique.

Development of LIPS sampling strategy and protocol for cortical and trabecular bone

LIPS analysis of the thin polished bone slides was executed in a predetermined fashion with respect to the region of interest (ROI) on the slides. ROIs representing cortical and trabecular bone areas were determined under microscope and clearly marked on the slides as segments (Fig. 1) or squares (Fig. 2) for segmental and matrix approaches, respectively. The

Table 1 The mathematical modelling of mineral constituents in the inorganic component of bone tissue

Minerals constituting the inorganic part	Mass % (MP)	Mineral density $\rho_{mineral}$	Density % (MP) × ρ	Chemical equation	Molecular weight (MW)	Molecular number (MN)	Molecular weight × molecular number (MW) × (MN)	Corrected molecular weight (CMW)	Weight % C_{oxide}
Calcite	0.0044	2.70	0.012	CaO	56.1	1	56.1	0.25	0.30
				CO_2	44.0	1	44.0	0.19	0.24
Hydroxyl apatite	0.4275	3.10	1.325	CaO	56.1	10	560.8	239.74	33.81
				P_2O_5	142.0	3	425.8	182.06	25.67
				H_2O	18.0	1	18.0	7.70	1.08
Magnesite	0.0071	3.00	0.021	MgO	40.3	1	40.3	0.40	0.74
				CO_2	44.0	1	44.0	0.44	0.81
Rock salt	0.0263	2.10	0.055	$NaCl$	102.9	1	102.9	2.71	2.52
	0.0003	1.99	0.001	KCl	119.0	1	119.0	0.04	0.02
Organic part	0.3990	1.60	0.638						29.17
Water	0.1354	1.00	0.135	H_2O	18.0	1	0.02	2.44	6.18
Total	1.0000		2.188			21	1429.04	435.71	100.00

See text for abbreviations

sampling strategy involved the consideration of the sampling system and sampling density. The ROI involved segmental and matrix networks, and when both types of networks were employed to execute the analysis, it was named as a combined sampling system.

In the *segmental* approach, the sample was analysed segmentally at 30 points indicated as blue lines in Fig. 1a. This figure shows sample B5. The slide was 100-μm thick and the two marked segments (S1 and S2) were 15 and 13 mm in length, respectively. The sampling density of these two segments were 0.5 and 0.3 mm, respectively (Fig. 1a).

A representative example of CaO concentration assessment using the segmental sampling approach (S1 and S2 in sample B5) is seen in Fig. 1b, c. CaO concentration values were calculated using the CaO calibration curve. Figure 1b, c show measurements along the S1 (mostly trabecular bone) and S2 (mostly cortical bone) segments, respectively. Osteoporotic areas are reasonably well demarcated and are associated with troughs in the corresponding CaO curves.

In the *matrix* sampling strategy, ROIs were marked as squares of 4 × 4 mm in size. LIPS measurements were performed in a 2-dimensional matrix of 10 segments and 10 sampling points in each segment. The sampling density was 300 μm. Thus, the total number of measurement points within this matrix was 100. Figure 2a illustrates the scanned picture of a representative sample (B1) showing the square ROIs.

CaO concentrations were also determined within these square regions representing the cortical and trabecular bone by LIPS (Fig. 2a). After measuring CaO concentrations in 10 points in 10 segments, the mean (±SD) CaO concentrations in the cortical and trabecular regions were 33.11 ± 3.99% (range 24.02–40.43%) and 27.60 ± 7.44% (range 3.58–39.51%), respectively. We also plotted the 100 CaO concentration values obtained from the cortical (Fig. 2b) and trabecular bone (Fig. 2c) on two-dimensional (2D) concentration distribution maps. Finally, we plotted CaO concentration distribution curves based on the actual values (Fig. 2d, e). Certainly, the cortical bone seems to be more homogeneous (Fig. 2)b, d. The mostly green colour seen in Fig. 2b indicates CaO concentrations between 25 and 40%. Only a very small area indicates CaO concentration above 40%. On the other hand, there is great heterogeneity in the trabecular bone (Fig. 2c, e) showing rather low (red-orange) and high (dark green) values. The very low values may correspond with Haversian canals.

As ICP-OES is a standard technique to assess element oxide concentrations in minerals, we sent our B1–B5 bovine bone samples to the laboratory of the GGIH. The homogenized bone powder was assessed by ICP-OES, and the CaO concentrations of the B1–B5 bone homogenates were 35.00, 33.26, 34.67, 34.52 and 35.03%, respectively (These values are similar to the ones obtained by our LIPS assessment: the CaO concentrations of the B1–B5 bones were 33.11, 30.68, 29.66, 24.55 and 28.89%, respectively (Table 3).

Table 2 Comparison of element oxide composition of bioapatite as determined by mathematical calculations versus published values [2]

Element oxide	C_o (%)	Elements	Constant	C_e (%)	Ca/P	C_e (%)*	Ca/P
	Mathematical modelling					Published data	
CaO	34.11	Ca	1.40	24.38	2.175	22.50	2.18
P_2O_5	25.67	P	2.29	11.20		10.30	
MgO	0.46	Mg	1.66	0.28		0.26	
NaCl	2.52	Na	4.47	0.56		0.52	
KCl	0.03	K	3.04	0.01		0.009	
CaF_2	0.00	F	2.05	0.00		0.005	
CO_2	0.75					3.50	
Water	7.28					6.00	

See text for abbreviations

C_o (%) element oxide concentration, C_e (%) Element concentration

We also wished to model how the measurement points would be located according to the structure of the bone. Based on data from literature [2], the calculated diameters (D) and areas (T) of the different structural units in bovine bone, such as osteon and Haversian canal. The estimated value of the approximately circular crater diameter (D) was 50 μm. As the shape of the crater is considered circular, the ablated area is:

$$T = 25^2 \times \pi = 1962.5 \ \mu m^2$$

If LIPS assessment of the *cortical bone* is performed according to the matrix sampling strategy (Fig. 1, segment S2), some measurement points may co-localize with either an osteon or a Haversian canal, depending on the sampling densit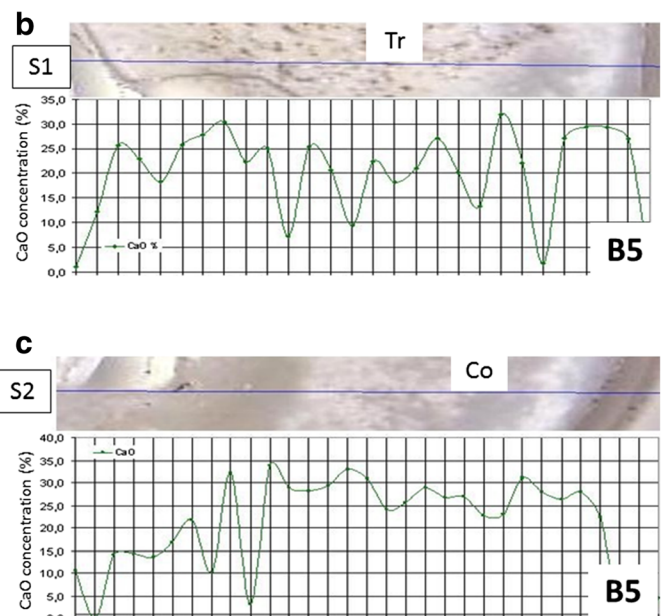y. With decreasing sampling density, the probability of targeting canals will increase. Thus, the inhomogeneity of the bones is well demonstrated by the CaO surface distribution diagram acquired by serial LIPS measurements performed along a 10×10 matrix as demonstrated above (Fig. 2). In this situation, the sampling density (distance of two adjacent measurement points) was 0.3 mm and the examined area was

$$(9 \times 0.3 \ mm)^2 = 7.29 \ mm^2.$$

Again, based on data from literature [2], the Haversian canal density per square millimetre is 3.65 in bovine bones. Thus, theoretically, there are $7.29 \times 3.65 = 26.6$ Haversian canals in the 7.29 mm² area covered by us. In Figs. 1 and 2, there are several areas with low CaO concentrations that may indicate Haversian canals.
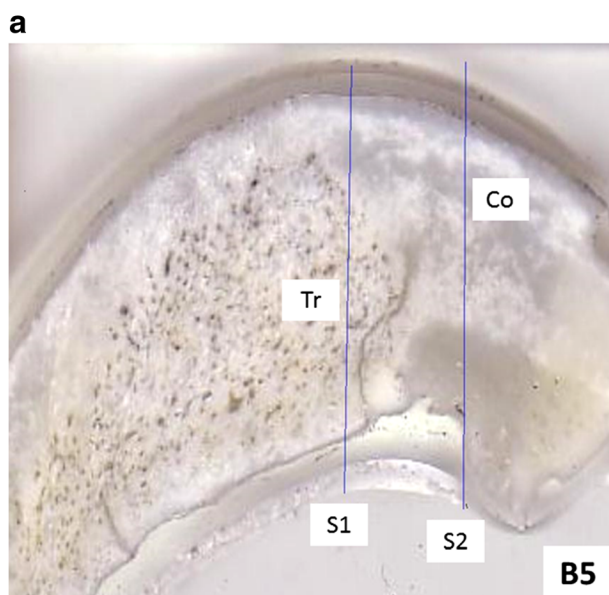
Fig. 1 CaO concentration assessment by segmental sampling approach. Two representative segments (S1 and S2) in sample B5 marked for segmented network LIPS analysis (**a**). CaO concentrations at various sampling points along the S1 (**b**) and S2 (**c**) segments. Both trabecular (Tr) and cortical (Co) bone could be assessed
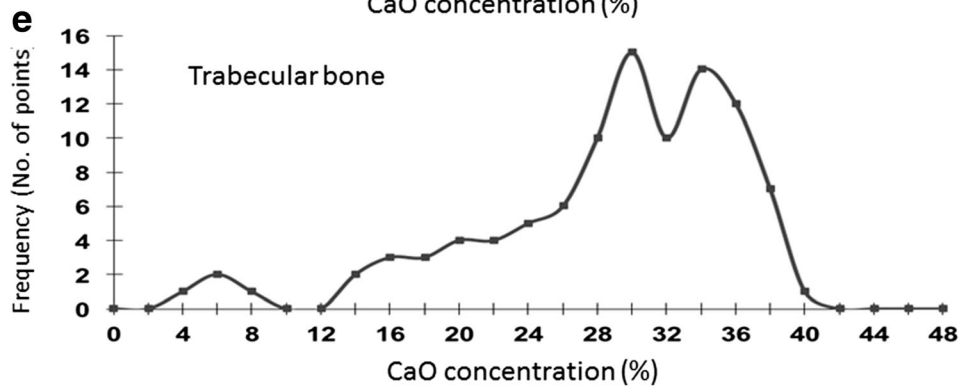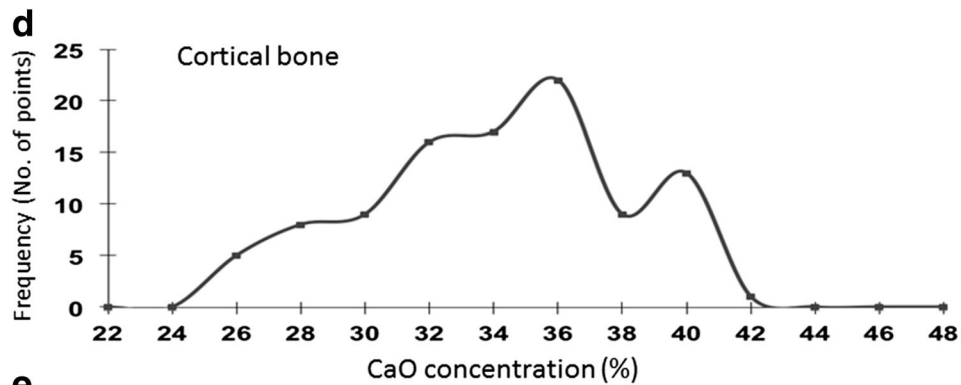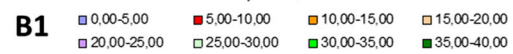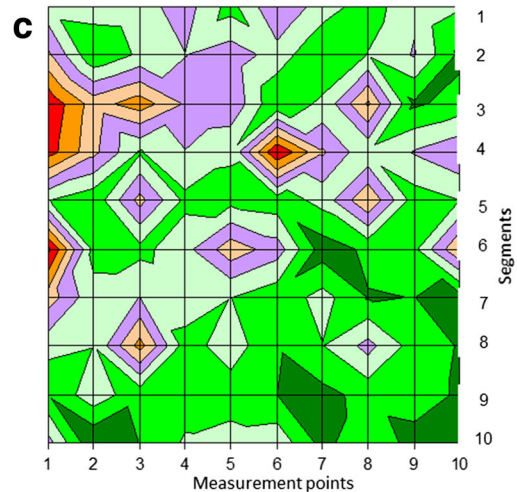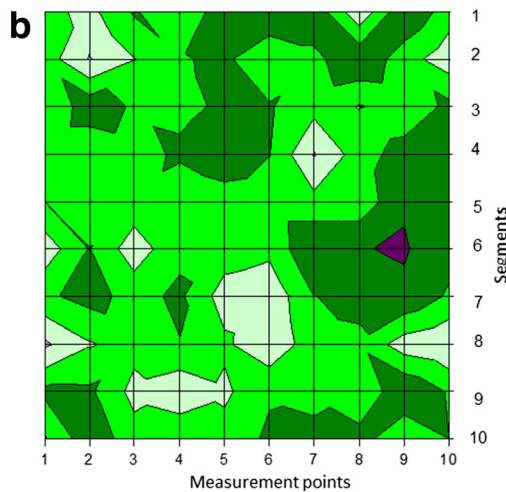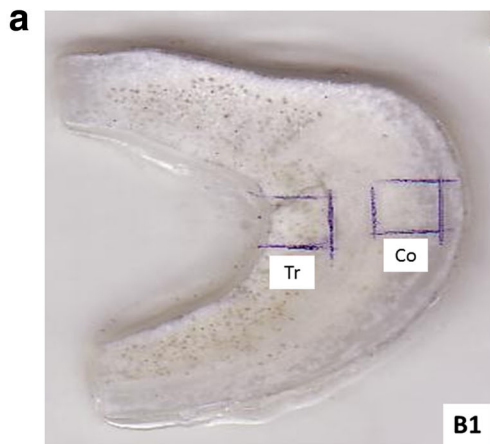
◄ Fig. 2 The matrix sampling approach. Region of interest (ROI) marking as squares on bovine bone slices. In sample B1, ROIs in the cortical (Co) and trabecular (Tr) bone regions were marked for LIPS analysis (**a**). CaO measurement value distribution in 10 segments and 10 measurement points in each segment in the cortical (**b**) and trabecular (**c**) area. The distance between any two measurement points (sampling density) is 300 μm. CaO concentration distribution curves in the cortical (**d**) end trabecular (**e**) bone

This situation may even be more complicated when the LIPS measurements are carried out in the *trabecular bone*. In living bone tissue, the trabecular part is interweaved with bone marrow and vessels. During the preparation of the sample for LIPS, the organic parts are removed by heating. Naturally, when LIPS measurements are conducted in the trabecular bone, more inhomogeneity of CaO distribution will be observed due to the thin bone lamellae and the large spaces in between (Fig. 1, segment S1) in comparison to cortical bone (segment S2).

Comparison of bovine bone density as determined by quantitative computed tomography and 'geological density' as measured by LIPS

Bovine bone samples were analysed by quantitative computed tomography (QCT) before slicing for LIPS. Results of QCT assessment of the B1–B5 bone samples are indicated in Table 4. The attenuation coefficient as determined by QCT may be one of the best determinants of altered bone tissue structure. First, we compared the QCT measured attenuation coefficient and total density and there was significant correlation between these two parameters (Fig. 3a).

We used a representative bovine bone sample (B2) for comparing bone density as determined by LIPS versus QCT. According to LIPS, the mean density of the B2 bone was 2.150 g/cm³. Significant correlation between QCT and LIPS density was found (Fig. 3b).

Table 3 CaO concentrations in B1–B5 bone samples determined by LIPS and ICP-OES

Bone homogenate samples	LIPS CaO (%)	ICP-OES CaO (%)
B1	33.11	35.00
B2	30.68	33.26
B3	29.66	34.67
B4	24.55	34.52
B5	28.89	35.03
Mean (μ_0)	29.38	34.50
Variance (σ_0)	3.13	0.72

Mathematical application of Bartlett's test to assess statistical homogeneity of bovine bones based on CaO content distribution

We can mathematically test bone homogeneity by matching the standard deviation (SD) values determined for element oxide content in bovine shin bones. First, we needed to determine whether the element oxide concentrations measured at individual locations exerted normal distribution or not. This hypothesis only works if element oxide levels exert a normal distribution.

We matched the SD values of concentration values determined in each section using the accepted 95% probability level. In statistics, Bartlett's test [33] is used to test if different samples are from populations with equal variances. In other words, Bartlett's test is used to test the null hypothesis that, in a given population, all variances are equal against the alternative that at least two are different [33]. We have previously used Bartlett's test in geological studies [34].

According to Bartlett's test:

$$K^2 = 2.3026/b \; k \; f_0 \left(\lg \sigma X^{(Pi) \times 2} - 1/k \sum \lg \sigma X^{(Pi) \times 2} \right)$$

where

b	Constant ($b = 1 + (k+1)/3kf_0$)
k	Number of segments
P_i	Sequence number of segments, where $i = 1, 2, 3 \ldots k$
n_j	Number of measurement points in one segment, where $j = 1, 2, 3 \ldots n$
f_0	Degree of freedom; $f_0 = n_j - 1$
X	Chosen element oxide (e.g. CaO)
$\sigma X^{(Pi)}$	Standard deviation (SD) of the mean concentration values determined for element oxide X, segment P_i
$\sigma X^{(Pi) \times 2}$	variance of the mean concentration values determined for element oxide X, segment P_i
$\lg \sigma X^{(Pi) \times 2}$	The base-10 logarithm of the squared SDs determined for element oxide X, segment P_i
$1/k \; \Sigma \lg \sigma X^{(Pi) \times 2}$	Mean of the base-10 logarithm of the SDs

This approach is proper if the samples contain at least four elements ($n_j \geq 4$). In our case, when using the matrix sampling strategy, the number of CaO concentration values, measured in individual segments, is $n_j = 10$ in each segment (Fig. 2).

If we determine a 95% probability level, before applying the Bartlett's test, first we need to define the K^2 values for all 10 segments and for all the 10 measurement points per segment. The mean and SD values will be used during the calculations. The summarized Bartlett's test results

Table 4 Results of QCT assessment of B1–B5 bone samples

Male bovine tibia samples		B1	B2	B3	B4	B5
QCT results	Total density (mg/cm^3)	270.1	617.3	684.4	552.7	796.9
	Trabecular density (mg/cm^3)	26.9	178.3	273.5	299.6	454.7
	Cortical density (mg/cm^3)	469.0	976.3	1020.4	759.6	1076.8
	Attenuation coefficient	0.237	0.329	0.338	0.181	0.376

based on our systematic LIPS network assessment of CaO carried out through trabecular and cortical areas of two representative bovine bone (B1 and B2) sample sections are shown in Table 5.

After obtaining the K^2 values as described above, we performed χ^2 test in order to complete homogeneity studies. We plotted the regression curve needed for the definition of the critical values χ^2 (0.95) corresponding to $f = k - 1$ degree of freedom and 95% critical level in the χ^2 test (not shown in figure). In Table 5, $P\ [K^2 < \chi^2\ (0.95)]$ is the probability value of a calculated K^2 value being lower or higher than the critical value corresponding to 95% probability and $f = k - 1$ degree of freedom. In bone samples where the calculated K^2 values are lower than the χ^2 (0.95) critical values corresponding to the $f = k - 1$ degree of freedom and 95% critical level (Table 5), we accept the hypothesis that the $\sigma X^{(Pi)}$ (=SD) values are similar and we consider the bone structure homogeneous. Bartlett's test results shown in Table 5 (k values, degree of freedom and probability [P] values) correspond to the crude measurement values. If there are outlier $\sigma X^{(Pi)}$ values, the sample cannot be considered homogeneous. As an example, very low CaO concentration (%) values are seen in the third

(5.71%) and sixth segment (3.58%) probably due to technical reasons. Originally, the number of segments (k) was 10. By deleting these two outlier segments, the corrected number of segments became 8. This enabled us to perform a corrected K^2 value calculations for eight segments. By filtering out the outliers, according to the repeated Bartlett's test, now even the trabecular bone could be considered homogeneous.

Homogeneity tests of bovine shin bones based on the CaO frequency curves

In addition to the Bartlett's test described above, we also used another statistical approach [35] in order to determined bone homogeneity based on the previous CaO frequency distribution curves. As an example, the crude values of CaO assessments in the cortical region of B1 and B2 bone samples, as well as the calculation are included in Table 6.

For the calculations, we assume that the probability variables in our samples follow normal distribution. Then, the CaO concentration range (r) was divided into 25 sections by taking 2% steps (1 to 46%) (Table 6). The calculated CaO concentration frequency values in the B1 and B2 samples are ν_i and μ_1, while the relative frequencies are ν_i/N and μ_i/M, respectively, where

$$N = \sum_{i=1}^{r} \nu_i \quad \text{and} \quad M = \sum_{i=1}^{r} \mu_i$$

If $N \to \infty$ and $M \to \infty$, then

$$\chi^2 = N \times M \times \sum_{i=1}^{r} (\nu_i/N - \mu_i/M)^2 / (\nu_i + \mu_i).$$

According to the values in Table 4, and using the regression curve described above,

$$\chi^2 = 100 \times 80 \times 4.18E{-}03 = 33.4.$$

This calculated χ^2 value is lower than the critical $\chi^2_{24}(0.95) = 36.6$ corresponding to degree of freedom $f = r - 1 = 25 - 1 = 24$ and to the 95% critical level. Thus, the cortical area of both B1 and B2 bone samples can be considered homogeneous with respect to CaO distribution.
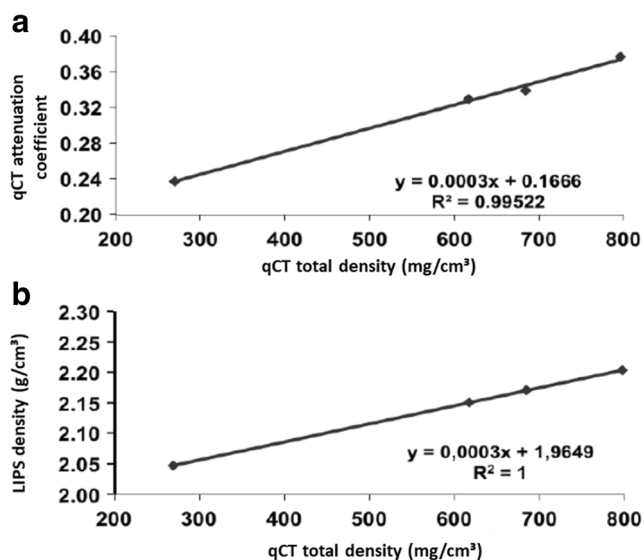
Fig. 3 QCT assessment of a representative bovine bone sample. Correlations between QCT total density and attenuation coefficient (**a**). Correlations between LIPS and QCT density values (**b**)

Table 5 Barlett's test results carried out on the standard deviation values of CaO assessment by LIPS in cortical and trabecular regions of the B1 bovine bone sample

Bone samples	Bartlett's test results					Bartlett's test corrected results				
	k	$f = k-1$	$f_0 = n_j - 1$	K^2	$P[K^2 < \chi^2(0.95)]$	k	$f = k-1$	$f_0 = n_j - 1$	K^2 (corrected)	$P[K^2 < \chi^2(0.95)]$
B1 cortical	10	9	9	6.625	16.90	10	9	9	6.625	16.90
B1 trabecular	10	9	9	25.233	16.90	8	7	9	13.996	14.10

k number of segment; n_j number of measurement points in one segment, where $j = 1, 2, 3 \ldots n$; f degree of freedom in the literature; f_0 degree of freedom in Bartlett's test; $P[K^2 < \chi^2 (0.95)]$ probability of $K^2 <$ critical value (see text for further explanation)

Table 6 Homogeneity assessment of the cortical region of the representative B1 and B2 bone samples using CaO distribution curves

r	Concentration range	Frequency and relative frequency of sampling values				$\frac{(\nu_i/N - \mu_i/N)^2}{(\nu_i + \mu_i)}$
		B1 cortical mesh		B2 cortical mesh		
	CaO[%]	ν_i	ν_i/N	μ_i	μ_i/M	
1	0	0	0	0	0	
2	2	0	0	0	0	
3	4	0	0	0	0	
4	6	0	0	1	0.0125	1.56E-04
5	8	0	0	0	0	
6	10	0	0	0	0	
7	12	0	0	0	0	
8	14	0	0	2	0.0250	3.13E-04
9	16	0	0	0	0	
10	18	0	0	0	0	
11	20	0	0	0	0	
12	22	0	0	3	0.0375	4.69E-04
13	24	0	0	1	0.0125	1.56E-04
14	26	5	0.0500	7	0.0875	1.17E-04
15	28	8	0.0800	17	0.2125	7.02E-04
16	30	9	0.0900	9	0.1125	2.81E-05
17	32	16	0.1600	16	0.2000	5.00E-05
18	34	17	0.1700	11	0.1375	3.77E-05
19	36	22	0.2200	6	0.0750	7.51E-04
20	38	9	0.0900	7	0.0875	3.91E-07
21	40	13	0.1300	0	0	1.30E-03
22	42	1	0.0100	0	0	1.00E-04
23	44	0	0	0	0	
24	46	0	0	0	0	
25	48	0	0	0	0	
		100	1.0000	80	1.0000	4.18E-03

r range division; ν_i and μ_1 frequency of sampling values; ν_i/N and μ_i/N relative frequency values

$$N = \sum_{i=1}^{r} \nu_i \quad \text{and} \quad M = \sum_{i=1}^{r} \mu_i$$

See text for further explanations

Conclusions

The possible similarities between the inorganic part of mineralized bone tissue and geological formations allowed us to use mathematical models when examining the mineral composition of bioapatite, the inorganic part of the bone tissue. The wt% of the element oxide composition in the inorganic part can be defined using these mathematical models.

The LIPS measurements conducted on bovine shin bone samples in a regular network, with sampling frequency of 300 μm, allowed us to define the concentration values of the element oxides, constituting bioapatite.

The interrelations between the sizes of the laser-induced craters during the LIPS measurements and the bone structure units, defined the distribution of individual elements, manifested by frequency distribution curves.

For the homogeneity testing of normal mineralized bone structure, we used two different statistical methods. During the Barlett's test, we used the equality of the SDs calculated for mean CaO content values. If the calculated K^2 values are lower than the critical χ_0^2 value corresponding to the degree of freedom $f = k - 1$ and to the 95% critical level, and if we accept the hypothesis related to the equality of SDs, the sample can be considered as homogeneous. The other method uses frequency distribution curves defined by statistical calculations. As an example, we compared the frequency distribution curve of two bovine bone samples. During these calculations, we found that the two cortical bone structures could be considered homogeneous with respect to CaO distribution. Otherwise, the deviations suggest changes in the bone structure and due to these changes, further tests are required in the future.

The described LIPS analysis and the mathematical calculations may enable us to assess CaO, as well as many other element oxides in bones, determine bone homogeneity and correspond bone structure changes with certain bone disorders.

Compliance with ethical standards

Conflict of interest The authors declare that they have no competing interests.

Ethical approval This article does not contain any studies with human participants or live animals performed by any of the authors.

References

1. Seeman E (2008) Bone quality: the material and structural basis of bone strength. J Bone Miner Metab 26(1):1–8
2. Skinner H (2013) Minerology of bone. In: Essentials of medical geology, Chapter 30, pp 665–685
3. Klein GL (2005) Aluminum: new recognition of an old problem. Curr Opin Pharmacol 5(6):637–640
4. Palacios C (2006) The role of nutrients in bone health, from a to Z. Crit Rev Food Sci Nutr 46(8):621–628
5. Malluche HH (2002) Aluminium and bone disease in chronic renal failure. Nephrol Dial Transplant 17(Suppl 2):21–24
6. Bervoets AR, Oste L, Behets GJ, Dams G, Blust R, Marynissen R, Geryl H, De Broe ME, D'Haese PC (2006) Development and reversibility of impaired mineralization associated with lanthanum carbonate treatment in chronic renal failure rats. Bone 38(6):803–810
7. Kazantzis G (2004) Cadmium, osteoporosis and calcium metabolism. Biometals 17(5):493–498
8. Shih RA, Hu H, Weisskopf MG, Schwartz BS (2007) Cumulative lead dose and cognitive function in adults: a review of studies that measured both blood lead and bone lead. Environ Health Perspect 115(3):483–492
9. Carmouche JJ, Puzas JE, Zhang X, Tiyapatanaputi P, Cory-Slechta DA, Gelein R, Zuscik M, Rosier RN, Boyce BF, O'Keefe RJ et al (2005) Lead exposure inhibits fracture healing and is associated with increased chondrogenesis, delay in cartilage mineralization, and a decrease in osteoprogenitor frequency. Environ Health Perspect 113(6):749–755
10. Mak TW, Shek CC, Chow CC, Wing YK, Lee S (1998) Effects of lithium therapy on bone mineral metabolism: a two-year prospective longitudinal study. J Clin Endocrinol Metab 83(11):3857–3859
11. Tannirandorn P, Epstein S (2000) Drug-induced bone loss. Osteoporos Int 11(8):637–659
12. Cohen O, Rais T, Lepkifker E, Vered I (1998) Lithium carbonate therapy is not a risk factor for osteoporosis. Horm Metab Res 30(9):594–597
13. Weinberg ED (2008) Role of iron in osteoporosis. Pediatr Endocrinol Rev 6(Suppl 1):81–85
14. Tapiero H, Tew KD (2003) Trace elements in human physiology and pathology: zinc and metallothioneins. Biomed Pharmacother 57(9):399–411
15. Lowe NM, Lowe NM, Fraser WD, Jackson MJ (2002) Is there a potential therapeutic value of copper and zinc for osteoporosis? Proc Nutr Soc 61(2):181–185
16. Kitchin B, Morgan SL (2007) Not just calcium and vitamin D: other nutritional considerations in osteoporosis. Curr Rheumatol Rep 9(1):85–92
17. Reginster JY (2007) Strontium ranlelate (Protelos). Rev Med Liege 62(11):685–687
18. Burlet N, Reginster JY (2006) Strontium ranelate: the first dual acting treatment for postmenopausal osteoporosis. Clin Orthop Relat Res 443:55–60
19. Ralston SH (2005) Bone densitometry and bone biopsy. Best Pract Res Clin Rheumatol 19(3):487–501

20. Griffith JF, Genant HK (2008) Bone mass and architecture determination: state of the art. Best Pract Res Clin Endocrinol Metab 22(5):737–764

21. D'Haese PC, Couttenye MM, Lamberts LV, Elseviers MM, Goodman WG, Schrooten I, Cabrera WE, De Broe ME (1999) Aluminum, iron, lead, cadmium, copper, zinc, chromium, magnesium, strontium, and calcium content in bone of end-stage renal failure patients. Clin Chem 45(9):1548–1556

22. Uryu T, Yoshinaga J, Yanagisawa Y, Endo M, Takahashi J (2003) Analysis of lead in tooth enamel by laser ablation-inductively coupled plasma-mass spectrometry. Anal Sci 19(10):1413–1416

23. Hetter KM, Bellis DJ, Geraghty C, Todd AC, Parsons PJ (2008) Development of candidate reference materials for the measurement of lead in bone. Anal Bioanal Chem 391(6):2011–2021

24. Liu G, Xie J, Liu X, Gao J (2002) Application of microwave dissolution and inductively coupled plasma-MS spectrometry for determination of ultra-trace level of lanthanides in human rib. Wei Sheng Yan Jiu 31(4):235–237

25. Raffalt AC, Andersen JE, Christgau S (2008) Application of inductively coupled plasma-mass spectrometry (ICP-MS) and quality assurance to study the incorporation of strontium into bone, bone marrow, and teeth of dogs after one month of treatment with strontium malonate. Anal Bioanal Chem 391(6):2199–2207

26. Shafer MM, Siker M, Overdier JT, Ramsl PC, Teschler-Nicola M, Farrell PM (2008) Enhanced methods for assessment of the trace element composition of iron age bone. Sci Total Environ 401(1–3): 144–161

27. Radziemski LJ (1994) Review of selected analytical applications of laser plasmas and laser-ablation, 1987-1994. Microchem J 50(3): 218–234

28. Maros G, Pasztor S (2001) New and oriented core evaluation method: ImaGeo. European Geologist 12:40–43

29. Maros G, Palotás K, Koroknai B, Sallay E (2002) Tectonic evaluation of borehole PTP-3 in the Krusné hory Mts. with ImaGeo mobile corescanner. Bull Czech Geol Surv 77:105–112

30. Maros G, Andrássy L, Zilahi-Sebes L, Máthé Z (2008) Modelling the boda aleurolite formation (BAF) based on core analyses using a laser-induced plasma spectrometer. First Break 26:143–154

31. Andrássy L, Zilahi-Sebess L, Vihar L (2003) Theoretical and statistical investigation of elemental concentration distributions determined by laser induced plasma atom emission spectra. Geophys Transact 44:95–138

32. Andrassy L, Maros G, Kovacs IJ, Horvath A, Gulyas K, Bertalan E, Besnyi A, Furi J, Fancsik T, Szekanecz Z et al (2014) Applicability of laser-based geological techniques in bone research: analysis of calcium oxide distribution in thin-cut animal bones. Orv Hetil 155(45):1783–1793

33. Bartlett M (1937) Properties of sufficiency and statistical tests. Proc Roy Stat Soc, Series A60(268–282)

34. Andrássy L, Maros G (2011) Statistical analysis of the distribution of element oxide concentrations measured by ImaGeo-LIPS in the boda siltstone formation. Magyar Geofizika (Hung Geophys) 52(2):62–79

35. Vincze I (1975) Mathematical statistics with industrial applications. Műszaki Könyvkiadó, Budapest